Supplemental to

Biokinetics and Dosimetry of [^{177}Lu]Lu-Pentixather and [^{90}Y]Y-Pentixather

Heribert Hänscheid[1], Andreas Schirbel[1], Philipp Hartrampf[1], Sabrina Kraus[2], Rudolf A. Werner[1], Hermann Einsele[2], Hans-Jürgen Wester[3], Michael Lassmann[1], Martin Kortüm[2], and Andreas K. Buck[1]

1) Department of Nuclear Medicine, University Hospital Würzburg, Würzburg, Germany
2) Department of Internal Medicine II, University Hospital Würzburg, Würzburg, Germany
3) Department of Pharmaceutical Radiochemistry, TU Munich, Munich, Germany

Administered activities

Activities and nuclides administered for pretherapeutic dosimetry and therapy of the patients included are listed in Supplemental Table 1. Dosimetry identified the kidneys as the dose-limiting organ. To be conservative, especially for the early therapies, activity was chosen to target at 23 Gy in the 1-mL volume with the highest activity concentration in SPECT/CT. Seven individuals remained untreated. Patient P5 became medically ineligible for therapy. Patients P11, P14, and P15 experienced unexpected problems with stem cell availability. Patients P17, P18, and P19 with solid tumors likely to require absorbed doses of several 10 Gy for effective therapy showed inadequate uptake into target tissue. All patients receiving therapy had hematologic neoplasms. Like the red marrow itself, degenerate hematologic cells in the medullary cavity, extramedullary lesions, and affected organs such as the spleen, if affected, are eliminated or at least significantly reduced at absorbed doses as low as 10 Gy and less.

Supplemental Table 1: Administered activities for pretherapeutic dosimetry and therapy

	Disease	Dosimetry (MBq ^{177}Lu)	Therapy (GBq ^{177}Lu)	(GBq ^{90}Y)
P1	Multiple myeloma	238	15.2	
P2	Multiple myeloma	199	23.5	
P3	Multiple myeloma	197	7.8	
P4	Multiple myeloma	206	9.9	
P5	Multiple myeloma	210	–	
P6	Multiple myeloma	210		6.2
P7	Multiple myeloma	197		2.2
P8	Multiple myeloma	209		5.0
P9	Multiple myeloma	207		4.9
P10	Acute myeloid leukemia	209		4.7
P11	Acute myeloid leukemia	203	–	
P12	Acute myeloid leukemia	205		5.6
P13	Diffuse large B-cell lymphoma	200		4.3
P14	Diffuse large B-cell lymphoma	212	–	
P15	pre-B acute lymphoblastic leukemia	212	–	
P16	T-cell leukemia	200		4.2
P17	Adrenocortical carcinoma	194	–	
P18	Adrenocortical carcinoma	216	–	
P19	Thymoma	199	–	

Supplemental Table 2: Absorbed dose estimates in organs without specific accumulation of Pentixather.

	Absorbed dose in Gy/GBq			
	Female		Male	
	Lu-177	Y-90	Lu-177	Y-90
Adrenals	0.09	0.52	0.08	0.57
Breast	0.06	0.22	0.05	0.18
Colon wall	0.05	0.15	0.05	0.12
Bone surface	0.24	0.72	0.19	0.56
Gallbladder wall	0.12	0.65	0.10	0.52
Heart wall	0.06	0.25	0.05	0.19
Lung	0.05	0.18	0.04	0.13
Oesophagus	0.06	0.20	0.05	0.15
Ovaries	0.07	0.22		
Pancreas	0.07	0.23	0.06	0.16
Prostate			0.06	0.21
Salivary glands	0.06	0.23	0.05	0.18
Skin	0.06	0.16	0.05	0.14
Small intestine wall	0.06	0.16	0.04	0.12
Stomach wall	0.06	0.25	0.05	0.14
Testes			0.05	0.18
Thyroid	0.06	0.21	0.05	0.17
Urinary bladder wall	0.08	0.75	0.07	0.62
Uterus/cervix	0.07	0.24		

Whole body scans

About 200 MBq ^{177}Lu-Pentixather without concomitant medication to protect the kidneys were administered to each patient for pre-therapeutic dosimetry. Activity kinetics were analyzed in whole body, kidney, liver, spleen, red marrow, and tumorous lesions. Patient imaging included a series of planar whole body scans and a SPECT/CT for normalisation to absolute activity concentrations.

All whole body scans were performed with the same dual head gamma camera (Siemens Symbia E, Siemens Healthineers, Erlangen, Germany) equipped with 15.9 mm thick scintillator crystals and medium energy collimators. Camera settings for whole body scans were 1024x256 acquisition matrix, 20% energy window at 208 keV, 10 cm/min scan speed, and identical measuring distance for all scans in a series.

All patients had whole body scans at 0.1 h, 4 h, 1 d, and 2 d post injection (p.i.) of the activity, all but 4 (P2, P5, P17, P19) at 1 h p.i., and 10 patients at 3 d p.i. (P1 to P5, P12 to P15, P18). The last scan was performed after 4 d except for P9 (5 d), P1 (6 d), and P4 and P14 (7 d). Supplemental Figure 1 shows a complete series of 7 whole body scans of patient P3.

Regions of interest (ROI) were drawn including the tissue under consideration, or part of the tissue in case of overlapping accumulating tissues, and over an area with representative background adjacent to the tissue ROI (Supplemental Figure 2).

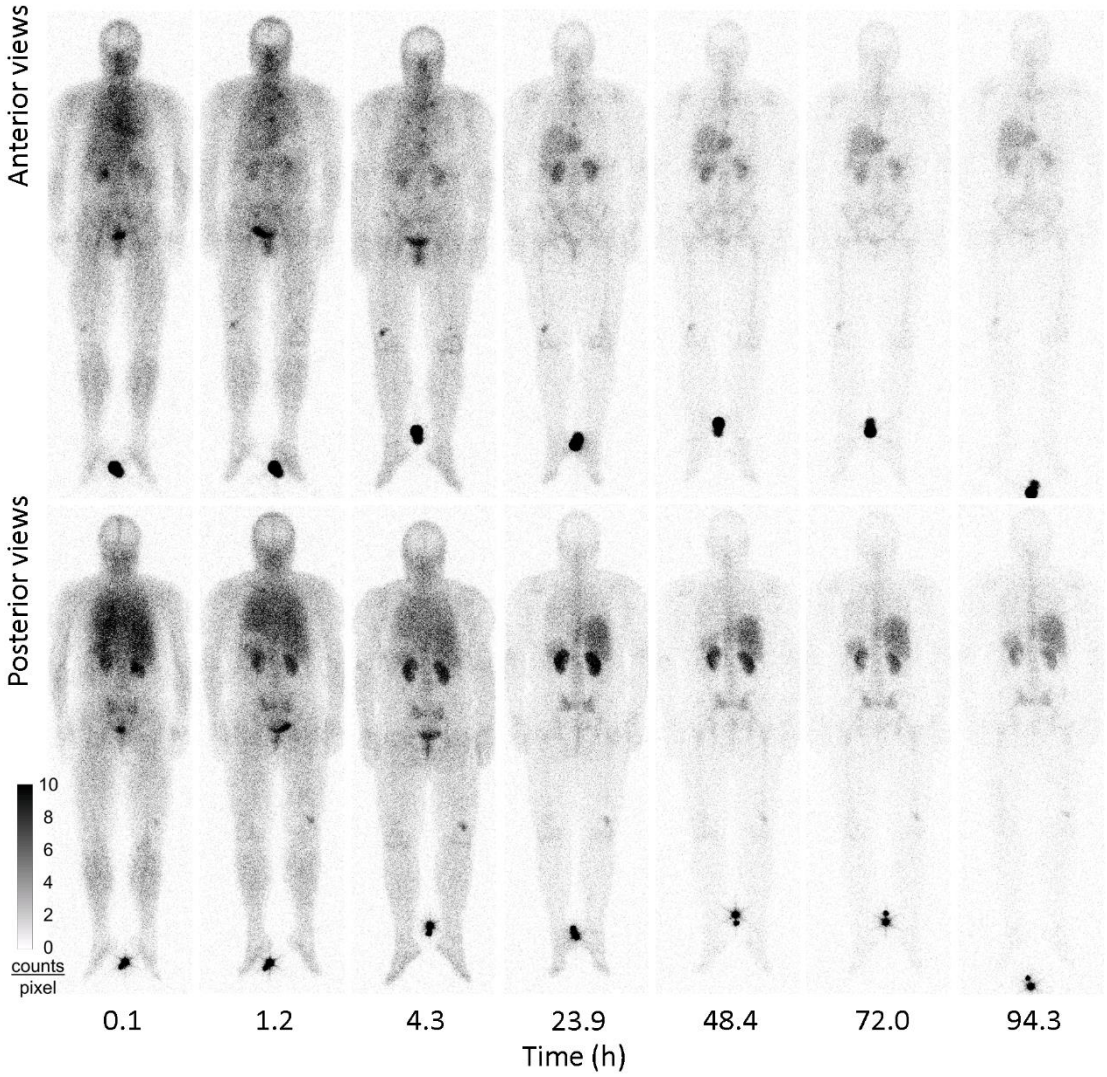

Supplemental Figure 1: Series of whole body scans of patient P3 after 197 MBq ^{177}Lu-Pentixather performed with the same gamma camera and identical camera settings, scan speed (10 cm/min), and measuring distance. The visible range of all images is 0 to 10 counts per pixel.

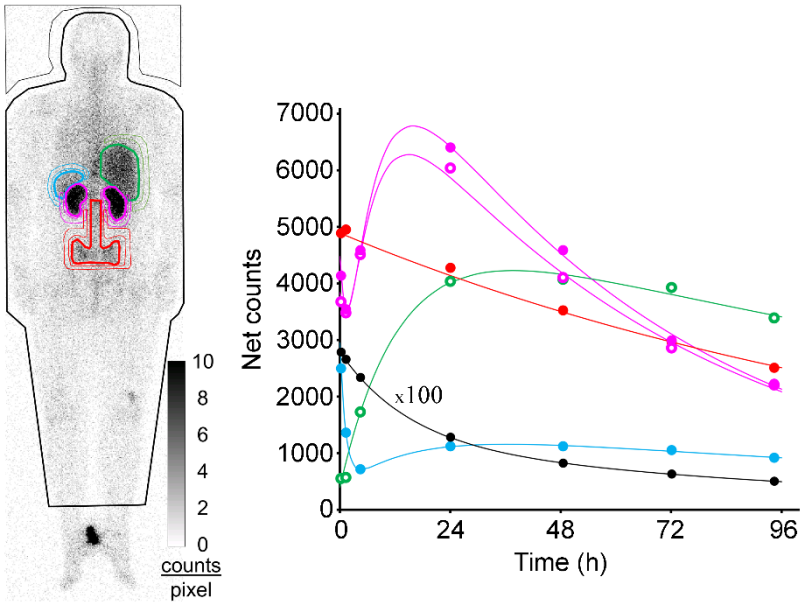

Supplemental Figure 2: Tissue and background ROIs in patient P3 and corresponding background-corrected net counts in the whole body (black dots), red bone marrow (red dots), liver (green circles), right (purple dots) and left (purple circles) kidneys, and spleen (blue dots) with respective fit functions. Whole body data were reduced by a factor of 100 for scaling.

Identical regions were copied to each scan in the series and background-corrected counts were extracted without further corrections e.g. for attenuation or scatter. While for kidneys, spleen, and red marrow net counts were derived from posterior images only, geometric mean of net counts in anterior and posterior views were calculated for the whole body and liver. The view used for lesions depended on the location and overlying accumulating structures. Given the long acquisition times, the net counts in the ROIs were found to be statistically sufficient to fit activity kinetics. For single kidneys, a median of 4980 net counts were registered in the scans after one day; 3 of 37 kidneys showed less than 2000 net counts (minimum: 932 in the right kidney of patient P15; Figure 1 in manuscript) and 3 more than 10000 net counts (maximum: 12248 in the right kidney of patient P19).

For most tissues, a bi-exponential decay function was fitted to the resulting net counts by ordinary least squares regression. Another short-lived exponential function was added when necessary to adequately reproduce the measured data up to 4 h (see spleen data in Supplemental Figure 2); the contribution to the integral under the curve, probably due to the perfusion effect, remained small in all cases. In the calculation of areas under the curves and from this time-integrated activity coefficients, the fit functions were assumed to be valid also for the time after the last measured value.

Tomographic imaging

The total body time-integrated activity coefficient was deduced by normalizing all net counts to those in the first scan at 0.1 h. For other tissues, kinetics were normalized to match the absolute activity uptakes measured one day (two days in patient P9) after the administration by SPECT/CT.

Tomographic images were acquired with a Siemens Symbia T2 or, in patients P1, P8, P12, P15, and P18 a Siemens Intevo Bold (Siemens Healthineers, Erlangen, Germany) over a rotation of 180° with 3° angular steps (= 2 x 60 frames) at 30 s per projection. For both dual head cameras used, data were acquired with medium energy collimators and a central 20% photopeak window at 208 keV between lower and upper 10% scatter windows. Data were reconstructed using an ordered subset expectation maximization algorithm with depth-dependent 3D resolution recovery (Siemens Flash-3D) with 6 subsets, 6 iterations, and a 6 mm Gauss filter for a 128x128 matrix with corrections for scatter and attenuation to obtain absolute activity quantification in voxels sized 0.11 cm^3.

For both cameras, the detection efficiency under the aforementioned imaging and reconstruction conditions was determined by measuring a large volume (6.9 L Jaszczak phantom) homogeneously filled with a known ^{177}Lu activity in a lutetium chloride carrier solution (10 µg inactive lutetium per g dissolved in 0.1 mol per L hydrochloric acid). Extensive measurements with phantoms of different volumes and shapes with and without scattering bodies and surrounding background activity indicated typical accuracies of 10% or less for volumes as large as human kidneys, where partial volume effects are of minor relevance.

Activity in accumulating tissues under consideration was typically entirely quantified in SPECT/CT by including all activity in a volume interest (VOI) defined by an isocontour that exceeded the tissue boundaries on CT by approximately 1 cm in all dimensions. Supplemental Figure 3 shows the boundaries of the VOIs in the pre-therapeutic SPECT/CT for the kidneys in patient P3.

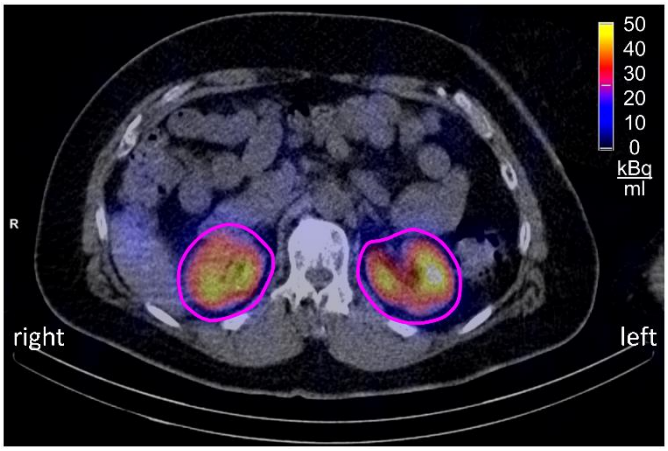

Supplemental Figure 3: Transverse plane of a SPECT/CT measured 24.7 h p.i. of 197 MBq ^{177}Lu-Pentixather in patient P3. SPECT image information was corrected for scatter and attenuation. Activity contents in the volumes of interest were 4.40 MBq for the left and 5.15 MBq ^{177}Lu for the right kidney.

Alternatively, in livers and enlarged spleens, where adjacent tissues with high activity concentration such as kidneys and tumorous lesions prevented the delineation of an isocontour VOI around the complete tissue, activity was quantified in a large subvolume within the organ and activity was scaled to the total mass measured by CT.

For the red bone marrow, the activity time function was determined in the planar images with a large ROI over pelvis and spine and normalized to the activity measured in SPECT/CT in L2-L4 in the lumbar spine, which was assumed to contain 6.7% of the total red marrow activity. In the absence of evidence of activity accumulation in bone, it was assumed that the measured activity was entirely located in bone marrow.

In order to estimate time-integrated activity coefficients, the activities measured by SPECT/CT were used for normalization of the kinetics deduced from the whole body scans. For example, activity in the right kidney of patient P3 was determined by SPECT/CT after 24.7 h to be 5.15 MBq ^{177}Lu corresponding to 2.23% of the administered activity. The fit function to the net counts of the right kidney in the planar whole-body scans (Supplemental Figure 2) indicated 6367 net counts after 24.7 h. The fit function to the net counts was normalized by a factor of 2.23% / 6367 to obtain the retention function shown in Figure 2 of the main manuscript, which was then integrated to calculate the time-integrated activity coefficient.

Uncertainties

The error to be assumed for the functions fitted to the whole body measurements depends on the kinetics and the uncertainty of the measured values. For the functions shown in Supplemental Figure 2, the fit yielded half-lives after ^{177}Lu-Pentixather of 47.5 h for the left kidney and 44.0 h for the right kidney. Assuming 5% relative error in single net count values and taking covariances into account, the statistical uncertainties are about 10% for the half-life values and about 5% for the areas under the curves. The uncertainties are about 15% and 7%, respectively, with 10% relative error in single net count values. Approximately one-third of the decays occur later than 72 h and one-fifth later than 96 h in a kidney with median kinetics parameters. Converted to ^{90}Y with its shorter physical half-life of 64 h, only about 17% of the decays occur later than 72 h and 9% later than 96 h.

The kinetics in tissues with long effective half-lives can be determined less accurately from measurements over four days. With 5% uncertainty in single net count values, the fit function shown in Supplemental Figure 2 for the liver corresponds to an effective half-live of 145 h ± 73 h for ^{177}Lu-Pentixather and 36% uncertainty of the area under the curve. Converted to the kinetics of ^{90}Y-Pentixather, the uncertainty of the area under the curve is reduced to 10%. The expected contribution from decays later than 96 h is 58% for ^{177}Lu and 23% for ^{90}Y in a liver with median kinetics parameters.

The error in activity measurement in tomography is derived from the calibration error, which is probably less than 10%, and statistical uncertainties in reconstruction and quantification. Measured ^{177}Lu activity concentrations in the right and left kidneys in our patients were in good agreement in most individuals. Only patients P17 and P18 with adrenocortical carcinoma showed large deviations with right to left activity concentration ratios of 1.36 and 0.70, respectively. In the other patients with two kidneys, this ratio was 1.03 ± 0.07, indicating typical statistical quantification errors in the order of 10%.

Post-therapeutic measurements

The first 4 patients P1 to P4 were treated with ^{177}Lu-Pentixather after pretherapeutic dosimetry (Supplemental Table 1). Except for P2 who received 23.5 GBq ^{177}Lu, these patients underwent a similar measurement program as in pretherapeutic dosimetry, but with shortened scan duration. The radiosynthesis for therapy followed the same protocol as for pretherapeutic dosimetry using higher amounts of Pentixather (200 µg) and gentisic acid (7 µg) per batch of 8 GBq $^{177}LuCl_3$.

Patient P3 received treatment with 7.8 GBq ^{177}Lu-Pentixather three weeks after pretherapeutic dosimetry, with whole body scans after 1, 4, 22, 48, 144, and 309 hours and SPECT/CT after 23 h. The posterior view acquired 1 day after the administration is shown in Supplemental Figure 4 together with the corresponding image from pre-therapeutic dosimetry. Data evaluation using the identical procedures as described above for pre-therapeutic dosimetry resulted in the retention values shown in Supplemental Figure 5.

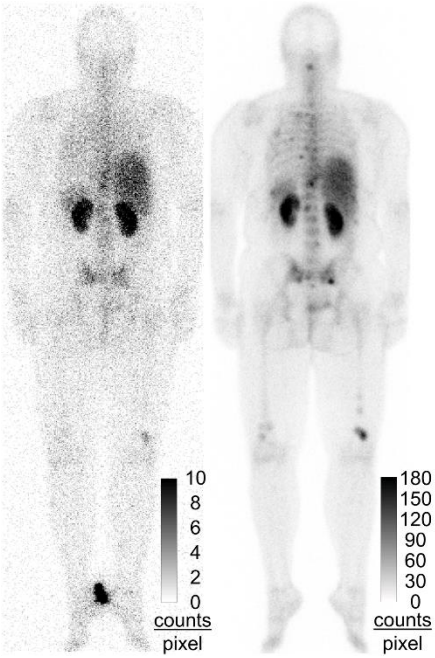

Supplemental Figure 4: Posterior whole body views of patient P3 24.1 h p.i. 197 MBq ^{177}Lu-Pentixather for pre-therapeutic dosimetry (left) and 22.2 h p.i. 7.8 GBq ^{177}Lu-Pentixather for therapy. Scanning speed was two times higher during therapy.

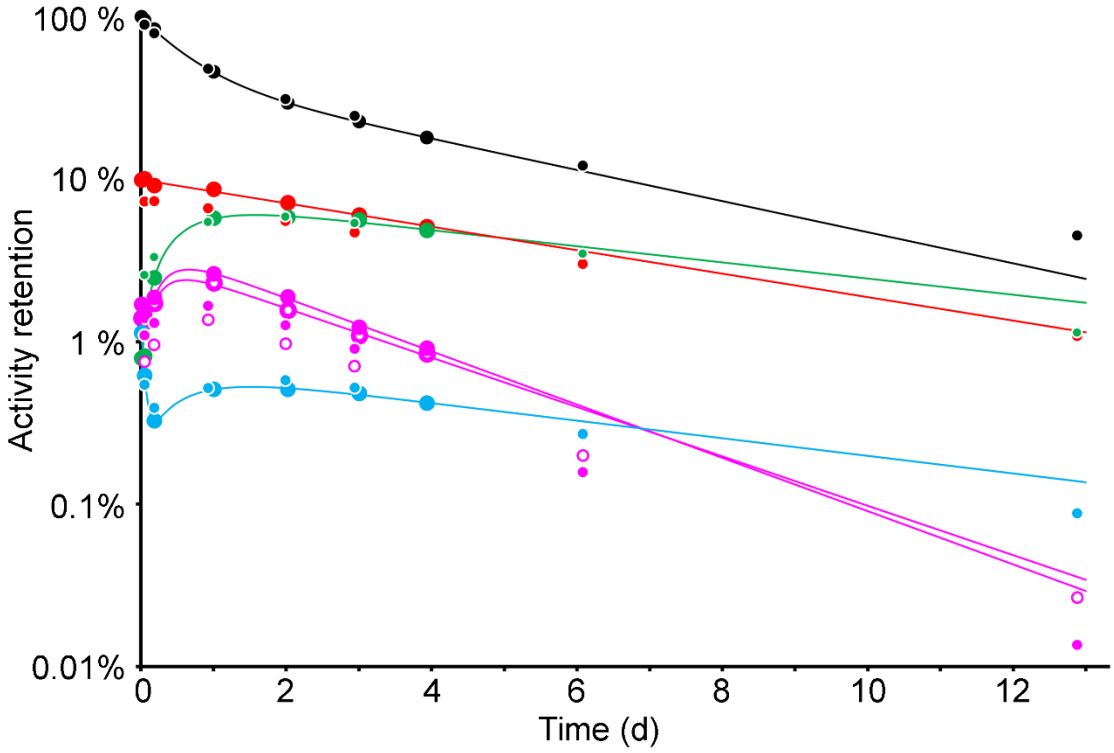

Supplemental Figure 5: Time functions of activity retention in the whole body (black dots), red bone marrow (red dots), liver (green dots), right (purple dots) and left (purple circles) kidneys, and spleen (blue dots) in patient P3. Large symbols indicate data measured after 197 MBq ^{177}Lu-Pentixather for pre-therapeutic dosimetry, small symbols data measured during therapy with 7.8 GBq ^{177}Lu-Pentixather. Solid lines show functions fitted to the dosimetry data and extrapolated to later times.

Retention values measured by SPECT/CT during therapy were 91 % of the corresponding pre-therapeutical values in liver, 99 % in spleen, 79 % in the spline, 60 % in left kidney, and 63 % in the right kidney. The shapes of the retention functions during therapy are generally well predicted by the dosimetric assessment, but the predictive power for late time points is limited, as expected.

Supplemental Table 3 lists the tissue absorbed doses per administered activity in patients P1, P3, and P4 with complete dosimetry after therapy with ^{177}Lu-Pentixather. Most time integrated activity coefficients are slightly reduced during therapy. Possible explanations are the higher injected activity and peptide mass during treatment and the altered clinical conditions such as an increased fluid intake and the infusion of amino acids. During dosimetry, no renal protective medication was administered because of the associated side effects.

The more pronounced reduction in retention in the kidneys suggests an effect of the amino acid infusion administered for renal protection. Since the effect of such a measure on a new radiopeptide cannot be easily estimated theoretically, the use of the medication was purely empirical with one of the most commonly used amino acid mixtures to competitively prevent reabsorption of the peptides in the renal tubules. To date, no attempts have been made to optimize the kidney protection medication for radiolabeled Pentixather.

Supplemental Table 3: Comparison of tissue absorbed doses per administered activity measured in pretherapeutic dosimetry and during therapy with ^{177}Lu-Pentixather in patients P1, P3, and P4. T/D indicates the averaged ratio of therapy to pretherapeutic dosimetry.

Patient	^{177}Lu-Activity	Kidneys (Gy/GBq)	Liver (Gy/GBq)	Spleen (Gy/GBq)	Red marrow (Gy/GBq)	Lesion (Gy/GBq)
P1	238 MBq	1.01	0.39	0.58	0.14	2.2
	15.2 GBq	0.59	0.38	0.49	0.11	2.5
P3	197 MBq	2.10	0.93	0.72	0.66	
	7.8 GBq	1.20	0.77	0.67	0.55	
P4	206 MBq	1.48	0.80	0.70	0.48	
	9.9 GBq	1.01	0.64	0.69	0.39	
T/D	51	61%	87%	92%	81%	114%